PASJ: Publ. Astron. Soc. Japan **55**, 191–202, 2003 February 25

Three-Dimensional Distribution of the ISM in the Milky Way Galaxy: I. The H I Disk

Hiroyuki NAKANISHI and Yoshiaki SOFUE
Institute of Astronomy, The University of Tokyo, 2-21-1 Osawa, Mitaka, Tokyo 181-0015
hnakanis@ioa.s.u-tokyo.ac.jp

(Received 2002 May 31; accepted 2002 November 8)

Abstract

We derived the three-dimensional distribution of H I gas in the Milky Way Galaxy using the latest H I survey data cubes and rotation curves. The distance of the H I gas was determined by the kinematic distance using a rotation curve. We solved the near–far problem in the inner Galaxy by a fitting method which involves introducing a model of vertical H I distribution. In our resultant maps we could trace three prominent arms: the Sagittarius–Carina arm, the Perseus arm, and the Outer arm. These three arms were found to be logarithmic spiral arms. The pitch angles of the Sagittarius–Carina, Perseus, and Outer arms were estimated to be about 11°, 18°, and 7°, respectively. The Sun is located in a region rich in H I gas between the Sagittarius–Carina arm and the Perseus arm. The H I disk shows large and asymmetric warping in the outer disk: the H I disk goes up to about 1.5 kpc above the Galactic plane in the northern hemisphere, and down to about 1 kpc in the southern hemisphere, which means asymmetric warping. The inner H I disk is also found to be tilting. The radius of the H I disk is about 17 kpc and the H I mass within this radius is estimated to be $2.5 \times 10^9\,M_\odot$, which corresponds to 1.5% of the dynamical mass predicted from the rotation curve. We also found that the H I outskirt is largely swelling in the fourth quadrant, and hence the Galaxy is significantly lopsided. The scale-height of the H I layer increases with the radius, and is correlated with the H I volume density at the centroid of the H I layer.

Key words: Galaxy: disk — Galaxy: kinematics and dynamics — Galaxy: structure — ISM: kinematics and dynamics — radio lines: ISM

1. Introduction

While the Milky Way Galaxy is the most explored galaxy, its global three-dimensional (3D) structure, such as the spiral arms, has not yet been clarified, because we are embedded in it. One of the best tracers of the global structure of the Galaxy is neutral hydrogen (H I) gas, because H I gas is one of the major components of the interstellar matter (ISM) in spiral galaxies, and the ISM is almost optically thin against the 21-cm line of the H I gas.

The earliest study of the global structure of the Milky Way using H I data was done by Oort, Kerr, and Westerhout (1958), who presented a face-on H I density map of the whole Galaxy. They reported several H I arms in the Milky Way: the so-called Sagittarius arm, the Orion arm, and the Perseus arm. Later, as more H I surveys were achieved, Kerr (1969), Weaver (1970), and Verschuur (1973) traced larger-radius H I arm, which is the so-called Outer arm, on a longitude–velocity diagram. Kulkarni, Blitz, and Heiles (1982) analyzed the H I data to make an H I density map for the outer Galaxy, and traced two arms having a pitch angle of $\sim 22°$–$25°$. Burton and te Lintel Hekkert (1986) showed three-dimensional H I maps of the outer Galaxy for all Galactic longitudes, and reported a warped H I disk. Diplas and Savage (1991) also presented an H I density distribution of the outer Galaxy, and discussed the warped disk and the flaring H I disk.

More recently, Hartmann and Burton (1997) archived a deeper and more complete survey with a much higher sensitivity. In the present work, we tried to convert this latest data cube into an H I distribution. Combining with the southern survey data cubes available, we aimed to derive a 3D map of the whole Galaxy. This paper is the first of a series presenting our analysis of the 3D structure of the ISM. In the second paper, we will present the result for molecular gas.

In this paper we describe the data and our method for deriving the H I distribution of the whole Galaxy in sections 2 and 3, and report on the resultant H I maps and some properties of the H I disk of the Galaxy in section 4.

2. Data

2.1. H I Survey Data

Three available H I survey data are used in this paper: the Leiden/Dwingeloo survey (Hartmann, Burton 1997), Parkes survey (Kerr et al. 1986), and NRAO survey (Burton, Liszt 1983), which all are archived in the FITS format. We took data within a latitude range of $-10° < b < +10°$ from these data cubes to study the H I distribution.

The Leiden/Dwingeloo survey (Hartmann, Burton 1997) is used for the northern hemisphere, which was obtained with the 25 m Dwingeloo radio telescope in the Netherlands with a half-power beam width (HPBW) of $0.^\circ6$. The data consists of 21 cm line spectra over the entire sky above declinations of $-30°$ with a grid spacing of $0.^\circ5$. The radial velocity (V_r) coverage is from -450 to $+400\,\mathrm{km\,s^{-1}}$ with a velocity resolution of $\simeq 1.03\,\mathrm{km\,s^{-1}}$. The r.m.s. noise level is 0.07 K. These spectra are averaged so that the bin width of latitude becomes 1° in this paper.

Table 1. Modified coefficients of the inner rotation curve.

	$R < 0.09\,R_0$	$0.09\,R_0 < R < 0.45\,R_0$	$0.45\,R_0 < R < R_0$
A_0	0.	325.0912	−2342.65649
A_1	3261.30	−264.0309	2663.95435
A_2	−17847.8	261.7602	−1156.07764
A_3	52752.5	−132.822906	269.354645
A_4	−87027.2	31.9537735	−36.2039909
A_5	74344.	−2.857958	2.8025787
A_6	−25510.	0.	−0.1158279
A_7	0.	0.	0.001977

The Parkes survey (Kerr et al. 1986) is used for the southern hemisphere, which was obtained with the CISRO 18 m telescope in Australia with an HPBW of 0.°8. It covers Galactic longitudes from $l = 240°$ to 350° with a grid spacing of $\Delta l = 0.°5$, and Galactic latitudes from $b = -10°$ to $+10°$, with a grid spacing of $\Delta b = 0.°25$. The velocity range is 300 km s^{-1} with a velocity resolution of $\simeq 2.1$ km s^{-1}. The average r.m.s. is 0.27 K. These spectra are also averaged so that the bin width of latitude becomes 1°.

The Galactic center H I survey of National Radio Astronomy Observatory is used for the southern hemisphere between $l = 350°$ and $l = 360°$ (Burton, Liszt 1983). This data cube was obtained with the 140-feet telescope of the NRAO, whose HPBW is 21′. The survey covers the region $348° < l < 10°$, $-10° < b < 10°$, and a grid spacing of 0.°5 in both l and b. The velocity range is $|v| < 310$ km s^{-1} and the velocity resolution is 5.5 km s^{-1}. The r.m.s. level is 0.03 K. These spectra are also averaged so that the bin width of latitude becomes 1°.

2.2. Rotation Curve

Since the 21-cm spectra have only information about the radial velocity of the H I gas, we need to transform the radial velocity, V_r, of the ISM in the Galaxy into the distance, r, in the line of sight. The relation between the radial velocity, V_r, and the distance, r, in the line of sight is obtained using the rotation curve of the Galaxy, assuming that it rotates circularly.

For the inner rotation curve, we use Clemens's rotation curve (Clemens 1985), which was derived from the Massachusetts–Stoney Brook Galactic equator CO survey. Clemens's rotation curve was fitted by a polynomial of the form

$$V(R) = \sum_{i=0}^{7} A_i R^i. \quad (1)$$

Though Clemens listed the fitted coefficients, A_i, for the cases of $(R_0, V_0) = (8.5$ kpc, 220 km s$^{-1})$ and (10 kpc, 250 km s^{-1}), we modified them for the case of $(R_0, V_0) = (8$ kpc, 217 km s$^{-1})$ in order to connect smoothly to the outer rotation curve in this paper. Modified coefficients are listed in table 1.

For the outer rotation curve, we use a model rotation curve of Dehnen and Binney (1998), which was determined by fitting to observational constraints ever obtained. However, because of the small number of data points for the outer rotation curve, the mass model has not been settled yet, and four types of models are presented by Dehnen and Binney (1998). Of the four models, Model 2 is adopted in this work, since it has the smallest deviation from the observation among the four. In using this rotation curve, we adopted $R_0 = 8$ kpc and $V_0 = 217$ km s^{-1}, which are used for the Galactic constant in Dehnen and Binney (1998). The shape of the whole rotation curve used in this paper is shown in figure 1.

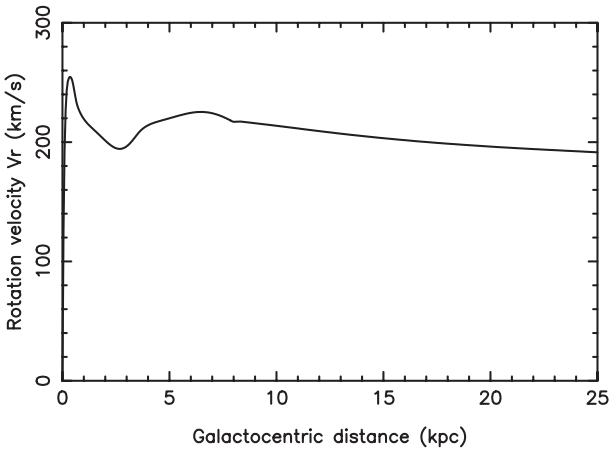

Fig. 1. Rotation curve used in this paper. The rotational velocity in the range of $R < 8$ kpc is cited from Clemens (1985), and that in the range of $R > 8$ kpc is cited from Dehnen and Binney (1998).

3. Method

In this section we describe a method for transforming the 21-cm spectra into an H I density distribution. Due to a geometrical reason, the H I distribution should be calculated separately in several cases: the outer Galaxy, the inner Galaxy, and near the tangential points. The radial velocity and the distance in a line of sight can be uniquely determined in the outer Galaxy, but the distance cannot be determined uniquely from the radial velocity in the inner Galaxy because of the near–far ambiguity. Since the H I gas has a velocity dispersion, the H I density at the tangential point cannot be calculated without considering its effects.

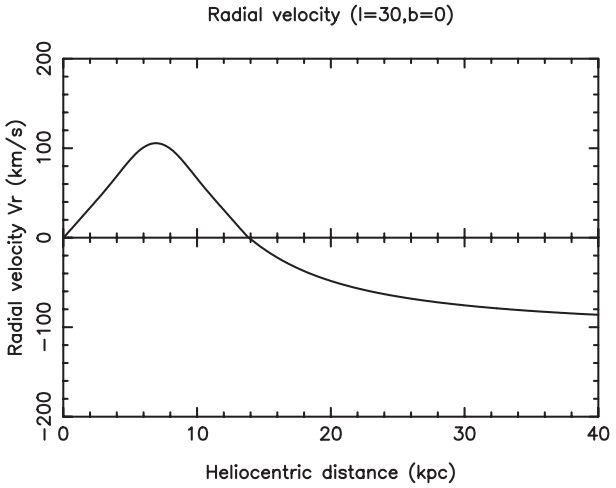

Fig. 2. Radial velocity versus the heliocentric distance in the direction of $l = 30°$ and $b = 0°$.

3.1. *Basic Idea and Derivation of the H I Distribution in the Outer Galaxy*

The distance of the H I gas having a radial velocity V_r can be calculated as follows. Assuming that the motion of the Galactic ISM is purely circular and that the gas away from the Galactic plane rotates at the same speed as the gas in the underlying disk, the radial velocity V_r of the ISM at Galactic longitude l, Galactic latitude b, and Galactocentric distance R is expressed by

$$V_r(l, b) = \left[\frac{R_0}{R}V(R) - V_0\right] \sin l \cos b. \quad (2)$$

The heliocentric distance r of the ISM at (R, l, b) is obtained by solving the equation

$$R^2 = r^2 + R_0^2 - 2rR_0 \cos l. \quad (3)$$

In the outer part of the solar orbit ($R > R_0$), we have one solution, $r = R_0 \cos l + (R^2 - R_0^2 \sin^2 l)^{1/2}$, because the other solution has a negative value, which is inadequate.

In the inner Galaxy ($R < R_0$) we have two adequate solutions, $r = R_0 \cos l \pm (R^2 - R_0^2 \sin^2 l)^{1/2}$; that is, we have the two-fold of kinematic distance in the inner Galaxy. However, at a tangential point where $R = R_0 \sin l$, equation (3) has only one solution despite the inner Galaxy. Hence, we have no ambiguity of distance at this point, and the kinematic distance is uniquely determined for a given radial velocity. For example, we plot the radial velocity against the heliocentric distance (r) in the case of $l = 30°$ in figure 2. The radial velocity in the longitude range $l < 90°$ becomes positive in the inner Galaxy, and increases toward the tangential point where it gets maximum. Beyond the tangential point it decreases monotonically and becomes negative in the outer Galaxy. The radial velocity for the whole Galactic equator is plotted in figure 3.

The H I density can be estimated as follows. If the 21-cm line is assumed to be optically thin, the H I column density N_{HI} [cm^{-2}] is given by integrating the brightness temperature, T_b [K], over the radial velocity, V_r [km s^{-1}],

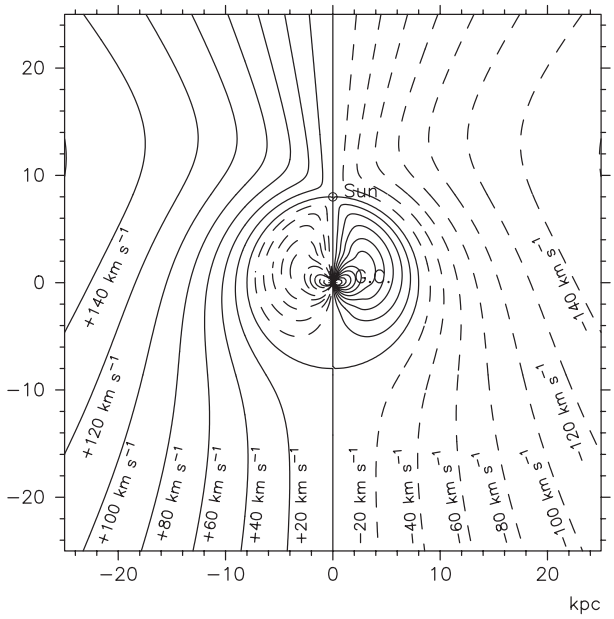

Fig. 3. Radial velocity field of the Galactic plane calculated with the rotation curve. The solid lines denote positive velocities and the dashed lines denote negative velocities.

$$N_{HI}\,[\mathrm{cm}^{-2}] = 1.82 \times 10^{18} \int_{V_{r_1}}^{V_{r_1}+\Delta V_r} T_b\, dV_r. \quad (4)$$

In this work, the velocity width, ΔV_r, is taken to be 2.06 km s^{-1} in the case of the Leiden/Dwingeloo survey, 2.00 km s^{-1} in the case of the Parkes survey, and 5.5 km s^{-1} in the case of the NRAO survey based on the velocity resolution of the southern survey.

The average volume density at an individual point is given by dividing the column density by the path length, Δr, which contributes emission in the velocity range $V_{r_1} < V_r < V_{r_1} + \Delta V_r$:

$$n_{HI}\,[\mathrm{cm}^{-3}] = \frac{N_{HI}}{\Delta r} = 1.82 \times 10^{18} T_b \frac{\Delta V_r}{\Delta r}. \quad (5)$$

Thus, we obtain the H I densities, n_{HI}, in the outer Galaxy from the 21-cm spectra $T_b(l, b, V_r)$. However, the local gas with a high velocity dispersion contributes to the high-altitude emissions. Therefore, the obtained H I distribution includes the local gas in the form of $n_{observed} = n_{HI} + n_{local}$. In this paper, we assumed that the local gas can be expressed by a linear function of the Galactic latitude, b, and subtracted it from $n_{observed}$. Because of this procedure, the diffuse H I gas, which extends to a high Galactic altitude (Diplas, Savage 1991), is subtracted, and can not be detected in the maps presented in this paper.

3.2. *H I Density around the Tangential Points*

At a tangential point $r = R_0 \cos l$ the kinematic distance can be uniquely determined even for the inner Galaxy. Since the H I gas has an intrinsic velocity dispersion, the H I spectra have a higher velocity component than the terminal velocity, V_t. The velocity dispersion, σ, is assumed to be 10 km s^{-1}; Malhotra (1995) estimated it to be 9.2 km s^{-1} for the first quadrant ($0° < l < 90°$), 9.0 km s^{-1} for the fourth quadrant

($270^\circ < l < 360^\circ$). In a given line of sight, the H I gas having a radial velocity of the range $|V_t| - \sigma \leq |V_r| \leq |V_t|$ contributes to a higher velocity component than the terminal velocity due the velocity dispersion. Also, equation (5) at the tangential points does not work because $\Delta V_r/\Delta r$ goes to zero there. Therefore, the volume density of the H I gas giving the radial velocity $|V_t| - \sigma \leq |V_r| \leq |V_t|$ around the tangential points is calculated by integrating the emission within the velocity range of $|V_t| - \sigma \leq |V_r| \leq \infty$, as follows:

$$n_{\rm HI}(r_t) = \frac{1.82 \times 10^{18} \int_{V_t-\sigma}^{\infty} T_b\, dV_r}{r_2(V_t-\sigma) - r_1(V_t-\sigma)}, \quad (0^\circ < l < 90^\circ), \tag{6}$$

$$n_{\rm HI}(r_t) = \frac{1.82 \times 10^{18} \int_{-\infty}^{V_t+\sigma} T_b\, dV_r}{r_2(V_t+\sigma) - r_1(V_t+\sigma)}, \quad (270^\circ < l < 360^\circ), \tag{7}$$

where $r_1(V_t \pm \sigma)$ and $r_2(V_t \pm \sigma)$ denote the heliocentric distances of the points giving radial velocities of $V_r \pm \sigma$. Subscripts 1 and 2 indicate the near and far points, respectively.

3.3. Derivation of the H I Distribution in the Inner Galaxy

In the inner Galaxy there are two points giving the same radial velocity in a given line of sight, and thus the observed spectra give the total emission at the near and far points. We solved this problem of the distance-degeneracy by considering the H I layer thickness.

First of all, we determined the H I layer thickness and its variations using the Galactocentric distance. For the model of the vertical distribution of H I we use Spitzer's model (Spitzer 1942). Spitzer (1942) analytically solved the dynamical z-distribution of stars and ISM. Assuming that the stars and gas in the Galactic disk are isothermal and self-gravitating, the number density $n_{\rm HI}$ can be expressed as a function of z by solving Poisson's equation in hydro-dynamical equilibrium. We then obtain

$$n_{\rm HI}(\xi) = n_{\rm HI0}\, {\rm sech}^2(\xi) \tag{8}$$

with ξ being

$$\xi = \log(1+\sqrt{2}) z - \frac{z_0}{z_{1/2}}, \tag{9}$$

where z is the height from the Galactic equator, $z_x 0$ is the height where $n_{\rm HI}$ becomes the maximum value ($n_{\rm HI0}$), and $z_{1/2}$ is the height where $n_{\rm HI}$ becomes half the value of the maximum, which is half the full width at the half maximum (FWHM).

In equation (8) we assume that $n_{\rm HI0}$ and z_0 vary with its position, but the scale-height, $z_{1/2}$, depends on the Galactocentric distance alone. We determined the H I layer thickness $z_{1/2}$ as a function of the Galactocentric distance by fitting the model function to the observed data. The thickness of the inner H I layer was determined by fitting the model function to the vertical distribution at the tangential point obtained in the previous section; we substituted the values into three parameters, ($n_{\rm HI0}$, z_0, and $z_{1/2}$) in equation (8), and chose the best set of parameters to fit to the observation by the least-squares method. The steps to search for the parameters were 0.001 of the peak for $n_{\rm HI0}$, and 1 pc for z_0 and $z_{1/2}$. On the other hand, the thickness of the outer disk was determined by fitting the model to all points, since there is no distance-ambiguity in the outer Galaxy. The resultant thickness of the H I layer is presented in figure 4.

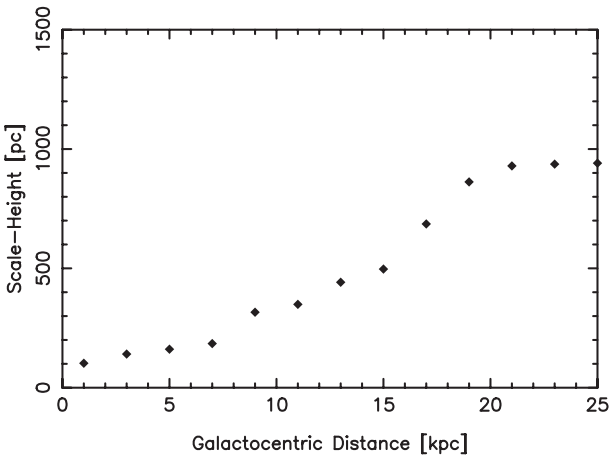

Fig. 4. Scale-height versus the Galactocentric distance.

For the next stage, the total emission was divided into two H I densities at the near and far points in the line of sight using the thickness of the H I layer. First, consider an H I gas having a radial velocity $V < V_r < V + \Delta V$ for a given longitude, l. This gas locates at corresponding kinematic distances, $r_1 - \Delta r_1/2 < r < r_1 + \Delta r_1/2$, and $r_2 - \Delta r_2/2 < r < r_2 + \Delta r_2/2$. Assuming that the H I gas follows Spitzer's model, the H I column density, $N_{\rm HI}(b)$, is represented as a function of latitude with four parameters: $n_{\rm HI0_1}$, $n_{\rm HI0_2}$, z_{0_1}, and z_{0_2}. That is,

$$N_{\rm HI}(b) = n_{\rm HI0_1}\, {\rm sech}^2(\xi_1) \times \frac{\Delta r_1}{\cos b} + n_{\rm HI0_2}\, {\rm sech}^2(\xi_2) \times \frac{\Delta r_2}{\cos b}, \tag{10}$$

where

$$\xi_1 = \log(1+\sqrt{2}) \frac{r_1 \tan b - z_{0_1}}{z_{1/2}}, \tag{11}$$

$$\xi_2 = \log(1+\sqrt{2}) \frac{r_2 \tan b - z_{0_2}}{z_{1/2}}. \tag{12}$$

The four parameters were determined by fitting the observed data by a model using the least-squares method. Finally, the H I density at the near and far points were calculated using ($n_{\rm HI0_1}$, z_{0_1}) and ($n_{\rm HI0_2}$, z_{0_2}), respectively.

3.4. Construction of the 3D H I Density Map

We thus obtain an H I density cube, $n_{\rm HI}(l, b, r)$, from the 21-cm spectra $T_b(l, b, V_r)$. Finally, the $n_{\rm HI}$ data cube in the (l, b, r) space was transformed into $n_{\rm HI}$ in (x, y, z) space where x, y, z are the Cartesian coordinates in the Galaxy. The position $(x, y, z) = (0, 0, 0)$ indicates the Galactic center (G.C.), and the Sun is situated at (0 kpc, 8.0 kpc, 0 kpc). The space of (l, b, r) was also transformed into cylindrical coordinates (R, θ, z), where R and θ are the distance from the rotation axis and the azimuth angle around it, respectively. The angle θ was taken so that $\theta = 180^\circ$ points to the Sun and $\theta = 90^\circ$ is parallel to $l = 90^\circ$.

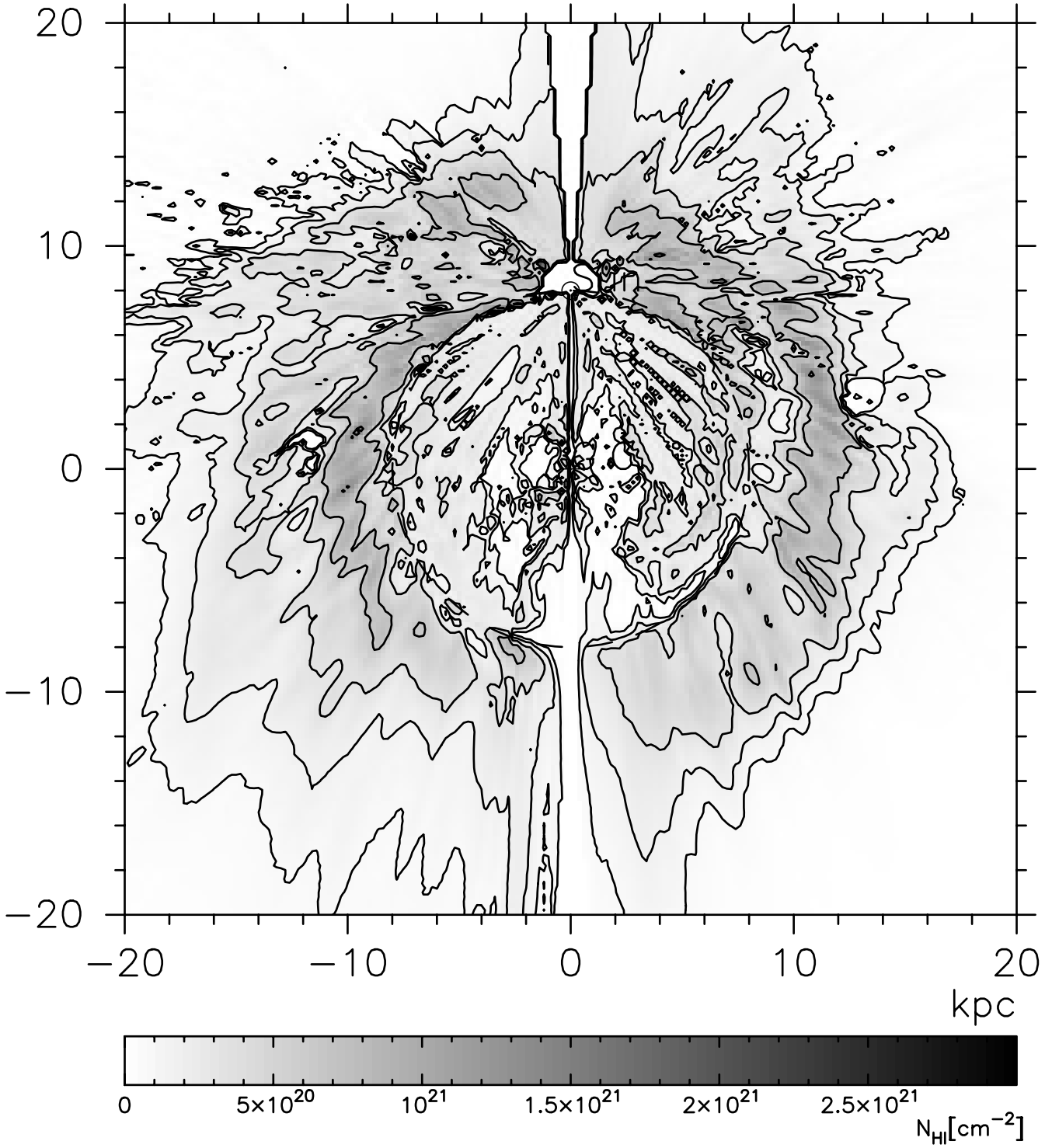

Fig. 5. H I column density map. The contours are drawn at levels of 8.0×10^{19}, 1.6×10^{20}, 3.2×10^{20}, 6.4×10^{20}, and 1.3×10^{21} atom cm^{-2}.

4. Results

The derived H I density distribution is presented in the forms of (1) a face-on H I column density map, (2) face-on H I volume density maps sliced at several altitudes, and (3) edge-on H I volume density maps sliced at several azimuthal angles around the Galactic center.

1. *Face-on column density map* — Figure 5 shows a face-on column density map of H I gas in the Galaxy. According to Spitzer (1942)'s model, the H I column density, Σ, is calculated

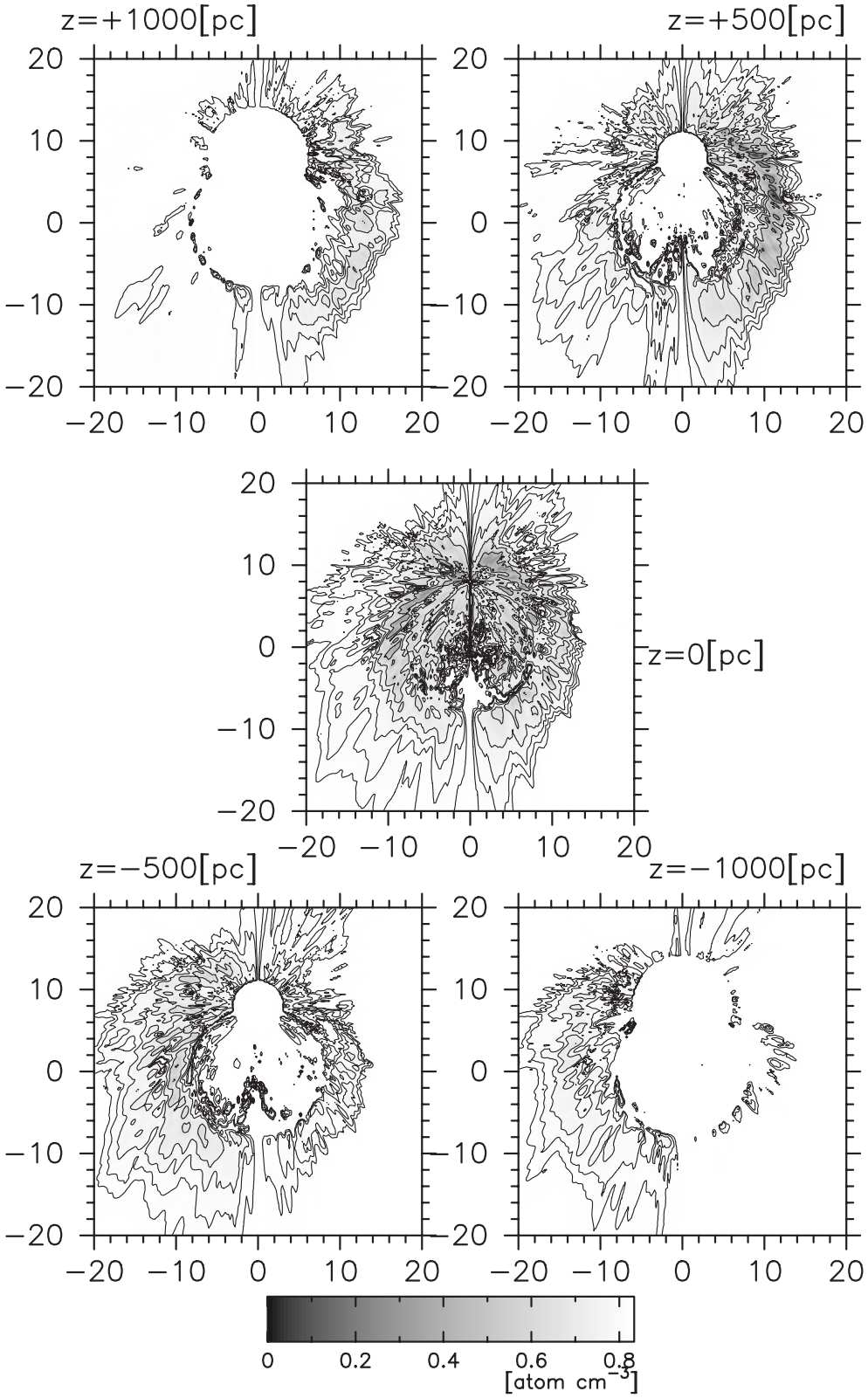

Fig. 6. Horizontal cross-section maps. Each map shows the H I volume densities in a sheet sliced parallel to the Galactic equator. The interval of each map is 500 pc; $z = +1000$ pc, $+500$ pc, 0 pc, -500 pc, and -1000 pc. The contours are drawn at levels of 0.01, 0.02, 0.04, 0.08, 0.16, 0.32, and 0.64 atom cm^{-3}.

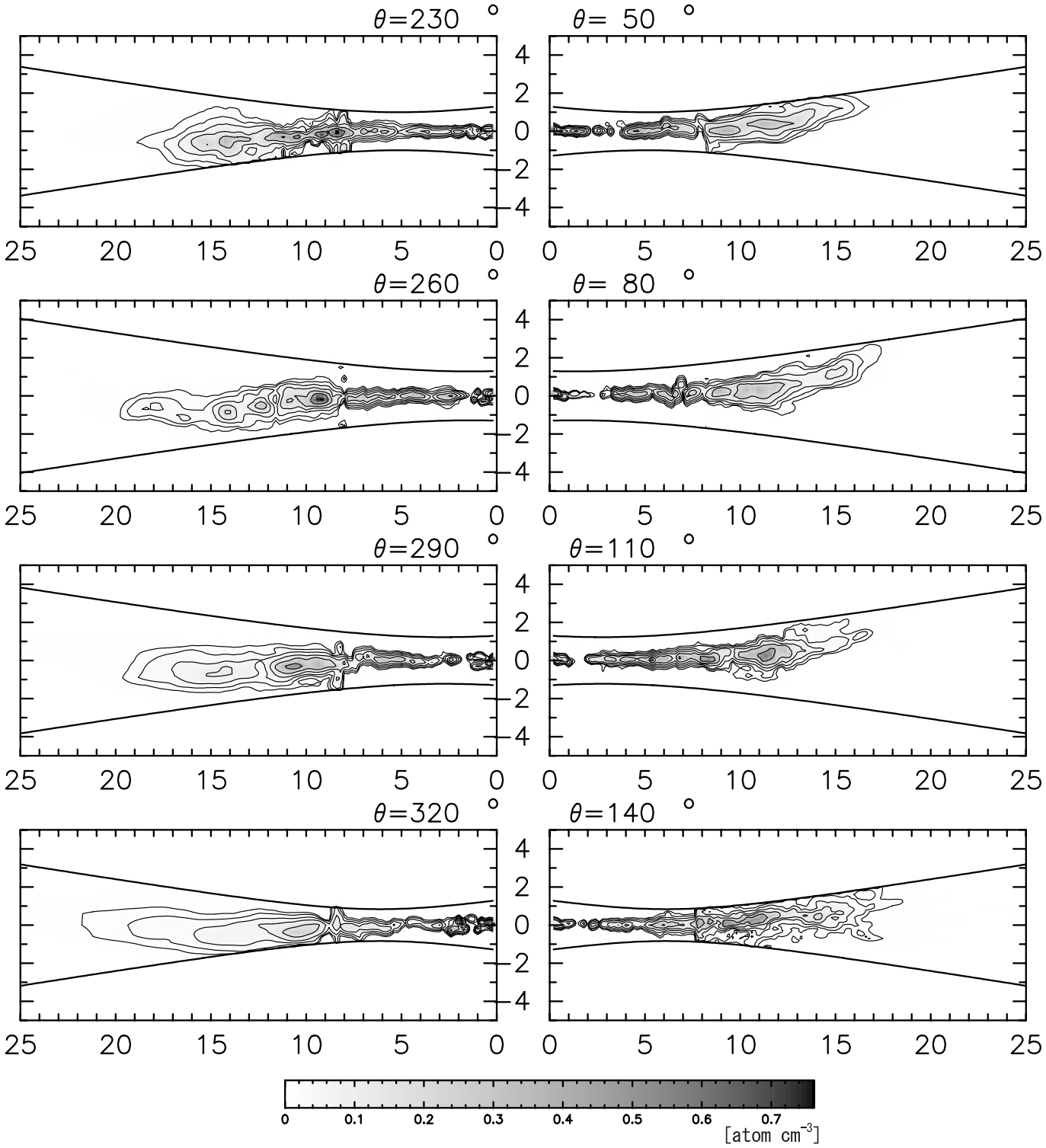

Fig. 7. Vertical cross-section maps. Each map shows the H I volume densities in a sheet through the Galactic center perpendicular to the Galactic plane. The individual panels show sections through $\theta = 50°$–$230°$, $\theta = 80°$–$260°$, $\theta = 110°$–$290°$, and $\theta = 140°$–$320°$. The contours are drawn at levels of 0.01, 0.02, 0.04, 0.08, 0.16, 0.32, and 0.64 atom cm^{-3}.

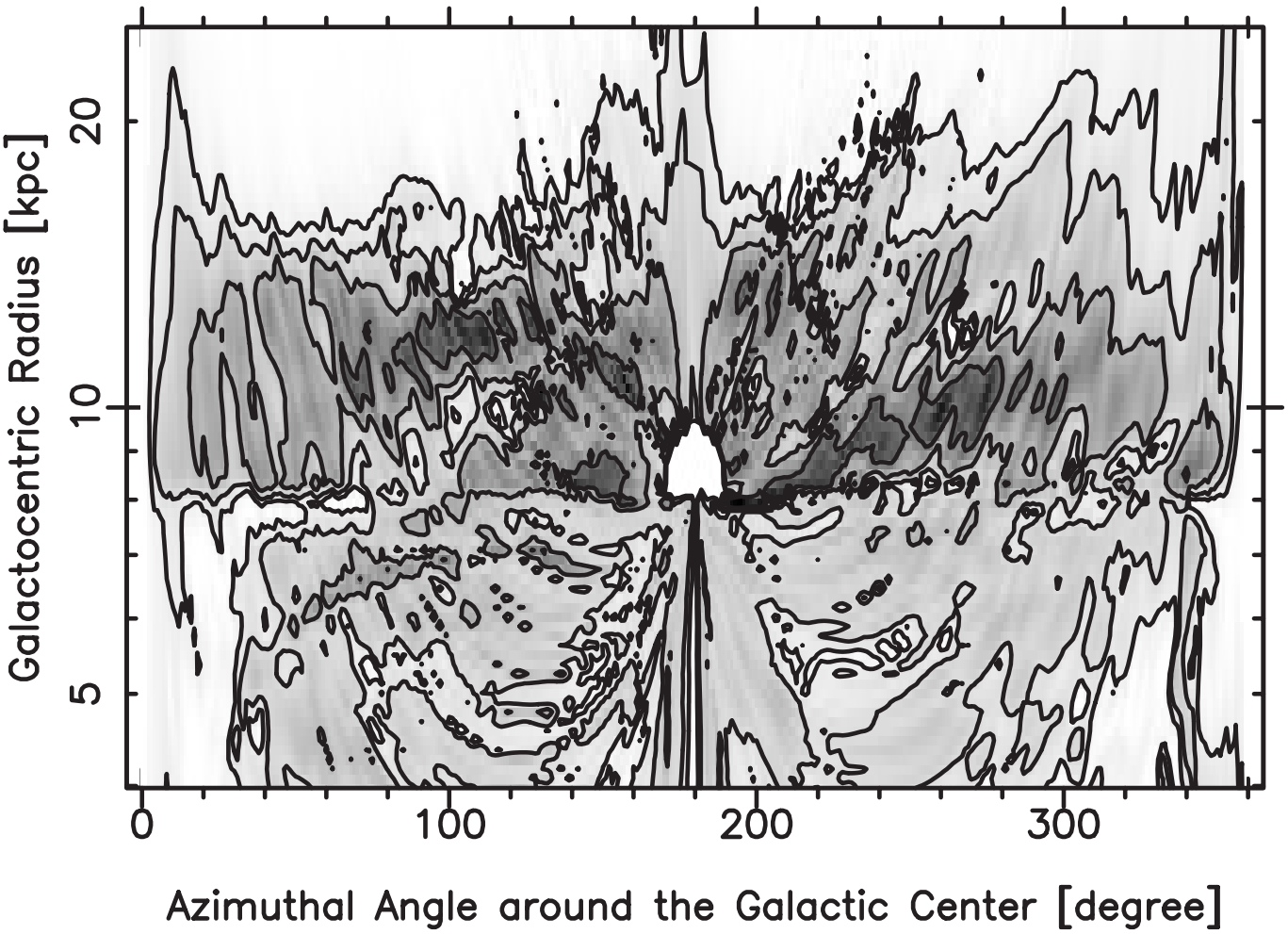

Fig. 8. H I column density map in polar coordinates. The vertical axis denotes the Galactocentric radius on the logarithmic scale, and the horizontal axis denotes the azimuthal angle around the Galactic center. The contours are drawn at levels of 1.0×10^{20}, 2.0×10^{20}, 4.0×10^{20}, 8.0×10^{20}, and 1.6×10^{21} atom cm^{-2}.

as

$$\Sigma(R,\theta) = 2.27 n_{\rm H10} z_{1/2}. \quad (13)$$

2. *Face-on volume density maps* — Figure 6 shows face-on volume density maps. Each map shows the H I volume densities in a sheet sliced parallel to the Galactic equator. The interval of each map is 500 pc; $z = +1000$ pc, $+500$ pc, 0 pc, -500 pc, and -1000 pc.

3. *Edge-on volume density maps* — Figure 7 shows edge-on volume density maps. Each map shows the H I volume densities in a sheet through the Galactic center perpendicular to the Galactic plane. Individual panels show sections through θ = 50°–230°, θ = 80°–260°, θ = 110°–290°, and θ = 140°–320°.

4.1. H I Spiral Arms

Some H I spiral arms can be traced in the resultant face-on maps, figures 5 and 6. In order to investigate the properties of the spiral arms, the H I column density is shown in polar coordinates in figure 8. The horizontal and vertical axes represent the azimuthal angle θ and the distance R from the Galactic center in logarithmic scale, respectively. Each arm on the polar diagram is found to be aligned in a straight line, indicating that the arms are logarithmic spiral arms. Schematic tracers of H I arms are presented in figure 9.

The largest arm is the so-called Outer arm which is traced from $(R,\theta) \sim (7.0\text{kpc}, -125°)$ to $(R,\theta) \sim (12.1\text{kpc}, 130°)$. The pitch angle is estimated to be $\sim 7°$. Another prominent arm is traced from $(R,\theta) \sim (5.6\text{kpc}, 100°)$ to $(R,\theta) \sim (11.4\text{kpc}, 310°)$, which is the so-called Sagittarius–Carina arm. Its pitch angle is also estimated to be $\sim 11°$. Another arm can be traced from $(R,\theta) \sim (5.8\text{kpc}, 50°)$ to $(R,\theta) \sim (13.6\text{kpc}, 200°)$, which corresponds to the so-called Perseus arm. The pitch angle is $\sim 18°$. This arm may apparently connect to the Outer arm (figure 5), but has a clearly different pitch angle. Hence, they may be distinct arms.

The Sun is located at a relatively H I-rich region between the Sagittarius–Carina arm and Perseus arm, which is called the local arm.

The Galactic spiral structure has been studied by many researchers using various methods. Oort, Kerr, and

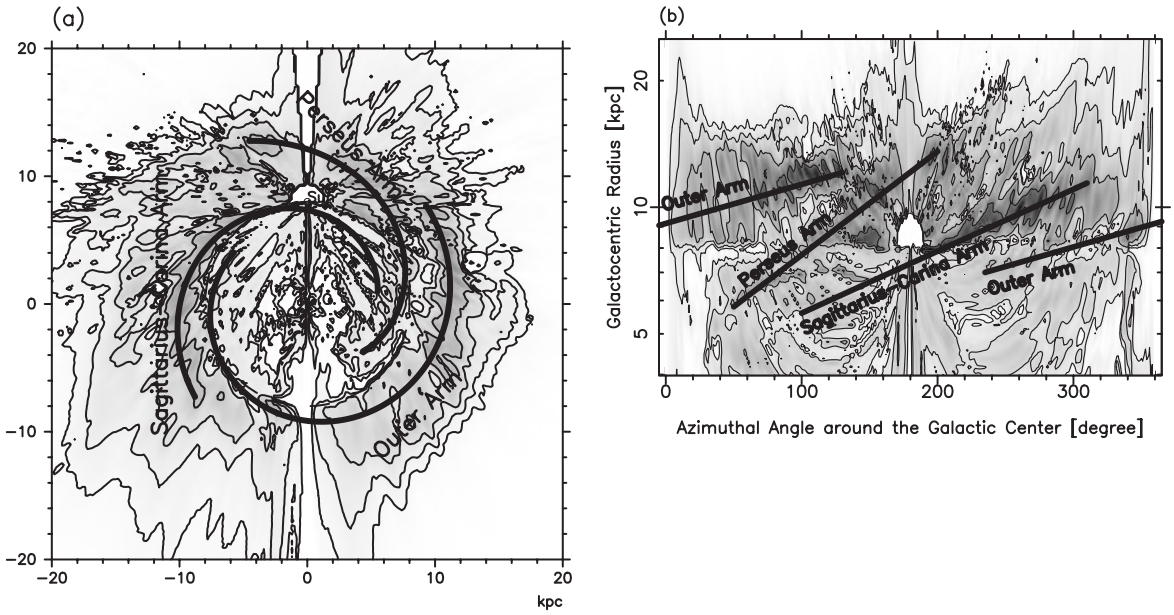

Fig. 9. (a) Schematic tracers of H I arms superposed on a resultant H I column density map. (b) Schematic tracers on a polar-coordinate diagram.

Westerhout (1958) found three H I spiral arms: the Sagittarius, Orion, and Perseus arms. Although the Orion arm may correspond to the local arm, the others are in good agreement with our traced arms. Weaver (1970) found the Outer arm, which also agrees with our result. They estimated the pitch angle of the Sagittarius–Carina arm to be 12.°5, which is consistent with our result. Kulkarni, Blitz, and Heiles (1982) reported three spiral arms, and estimated the pitch angles to be 22°–25°, which are pretty large compared to our values. Georgelin and Georgelin (1976) presented four spiral arms using the H II regions. They traced the Sagittarius–Carina arm with a pitch angle 10°–15°, and the Perseus arm with a pitch angle of 11°, which are consistent with our results. However, their Scutum–Crux and Norma arms could not be confirmed in our H I map. Drimmel and Spergel (2001) fitted the far and near infrared data form COBE/DIRBE by a 2- and 4-armed logarithmic spiral model. Our Sagittarius and Perseus arms are consistent with their spiral structure. Also, our result that the Galactic arms are logarithmic spiral arms confirms their logarithmic spiral model.

4.2. *Size and Mass of the H I Disk*

The radial distribution of the surface density of the H I gas is shown in figure 10 by averaging it azimuthally. The surface density is low near the Galactic center, and is lower than $1.9\,M_\odot\,\mathrm{pc}^{-2}$ within a radius of 6 kpc. The H I surface density attains the maximum values at radii of 7–12 kpc, where it becomes larger than $4\,M_\odot\,\mathrm{pc}^{-2}$. Then, the H I density decreases toward the outer region. It amounts to $\sim 1\,M_\odot\,\mathrm{pc}^{-2}$ at a radius of 17 kpc, and therefore the size of the H I disk is 17 kpc according to the definition of Broeils and van Woerden (1994). This radius of the H I disk is about 1.3-times as large as the stellar disk, since the stellar disk is estimated to be 13 kpc assuming $R_0 = 8$ kpc (Robin et al. 1992). This ratio is typical for general spiral galaxies.

The H I mass within a radius of 17 kpc was calculated to be $2.5 \times 10^9\,M_\odot$, which corresponds to 1.5% of the total mass predicted by the rotation curve.

4.3. *Warping and Tilting H I Disk*

Figure 7 shows that the H I disk is strongly warping at the outer region, which is consistent with former studies (Burton, te Lintel Hekkert 1986; Diplas, Savage 1991). The amplitude of warping is large in the directions $\theta = 80°$ and $\theta = 260°$. In the direction $\theta = 80°$, warping starts near $R = 12$ kpc, and the H I disk is bending up to $z = +1.5$ kpc height from the Galactic plane at $R = 16$ kpc. Also, in the direction of $\theta = 260°$, warping also starts at $R = 12$ kpc. Then, the H I disk is bending down to $z = -1$ kpc height from the Galactic plane at $R = 16$ kpc, and is flopping back to $z = -0.5$ kpc height at $R \sim 18$ kpc. Thus, the Galactic warping is found to be asymmetric. Since the size of the stellar disk is thought to be about 13 kpc, the warping starts at the edge of the stellar disk, which follows one of the rules of warping (Binney 1992). Hence, the warping is asymmetric.

This work displays the tilting of the inner disk (Burton, Liszt 1978; Sanders et al. 1984). In figure 11, the centroid of the H I disk z_0 at $R = 5$ kpc is plotted versus azimuthal angle θ for an instance, which shows that the H I disk is tilted against the $b = 0°$ plane. The amplitude of the tilting is ~ 100 pc. The H I disk is bending up in the direction $\theta \sim 80°$, and is bending down in the direction $\theta \sim 260°$, which is the same trend as the warping of the outer disk.

4.4. *Lopsided H I Disk*

Figure 5 shows that the Galactic H I disk is not symmetric. The H I disk is swelled in the direction $\theta = 310°$ in the third quadrant. The radius of the outer H I disk (defined by the contours at $8.0 \times 10^{19}\,\mathrm{H\,cm}^{-2}$ in the second quadrant) is ~ 11 kpc, whereas it is ~ 22 kpc in the fourth quadrant. Hence, the Galaxy is significantly lopsided in H I.

4.5. *Scale-Height of the H I Disk*

We define the scale-height of the H I disk as the value of $z_{1/2}$ (see subsection 3.3). The azimuthally averaged scale-height is plotted in figure 4 versus the radius. Figure 4 shows that the scale-height increases with radius, from ~ 100 pc at $R = 1$ kpc to ~ 700 pc at $R = 17$ kpc. According to Spitzer (1942)'s model, the scale-height is calculated as

$$z_{1/2} = 0.274 \sqrt{\frac{2\sigma^2}{3\pi G\rho}}. \quad (14)$$

Assuming that velocity dispersion is constant at any radius, the increase in the scale-height implies a decrease in the surface mass density at the Galactic plane.

In subsection 3.1, the volume density of H I gas ($n_{\rm HI0}$) and scale-height ($z_{1/2}$) are obtained for each point of the outer Galaxy. In figure 12, we plot the scale-height, $z_{1/2}$, versus H I volume density, $n_{\rm HI0}$, in an annulus of a constant radius of $R = 12.0 \pm 0.5$ kpc. Figure 12 shows that there is a negative correlation between the H I volume density, $n_{\rm HI0}$, and the scale-height, $z_{1/2}$, which were determined independently of each other in our analysis. The H I volume density is approximately expressed by $n_{\rm HI0} = 0.63 \exp(-z_{1/2}/340\,{\rm pc})$ by a least-squares fitting.

4.6. *Possible Systematic Problems*

In this work, resultant maps were obtained based on some assumptions, which might potentially cause systematic errors in our results. Possible systematic problems are described below.

1. *Pure circular rotation* — Though the distances of H I clouds were calculated based on an assumption that the Galaxy rotates in pure circular rotation, Burton (1972) mentioned that the streaming motion predicted by the density wave theory is not negligible. However, because we are interested in the global distribution of the H I gas, the effects due to the streaming motion were not taken into account. Since the streaming amplitudes were estimated to be between 3 and 8 km s^{-1}, the typical errors in the calculated distances of H I clouds were on the order of 1 kpc. Particularly, in the central region, the non-circular motion may be large, because the Galaxy is believed to have a bar whose size is estimated to be about 3 kpc. Hence, the H I distribution in the central 3 kpc may be incredible.

2. *Dependence on rotation curves* — Our resultant H I map is dependent on the rotation curves and there occur two possible systematic errors. First is the H I disk size. If the rotation velocity is larger than the one we used, the H I disk will be stretched outwards. Second is the H I contrast. If a rotation curve has multiple peaks such as those found in rotation curves of Honma and Sofue (1997), H I is concentrated in rings at corresponding radii, because the H I density depends on $|dV_{\rm r}/dr|$ in equation (5). We used a smooth rotation curve in order to avoid such artificial rings.

3. *Cylindrical rotation* — We assumed that the gas away from the Galactic plane rotates at the same speed as the gas in the underlying disk. This assumption was often used in former studies (Lockman 1984; Diplas, Savage 1991). However, this assumption may not be adopted for the high-altitude H I gas, because it is known that the rotation velocity at a large distance from the Galactic plane becomes slower than that of the gas at the underlying disk (Swaters et al. 1997) based on observations of an external edge-on galaxy, such as NGC 891 in H I line.

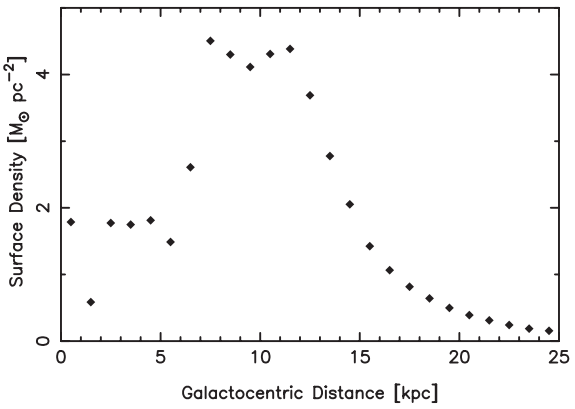

Fig. 10. Surface density of the H I gas versus the Galactocentric distance.

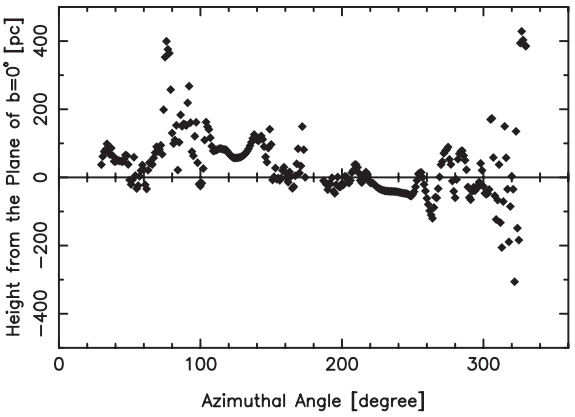

Fig. 11. Plots of centroid z_0 of the H I disk versus the azimuthal angle θ around the Galactic center at $R = 5$ kpc.

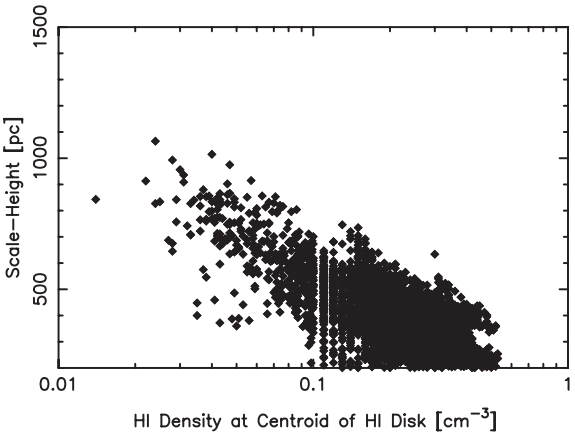

Fig. 12. Changes in the scale-height at an annulus of constant radius $R = 12.0 \pm 0.5$ kpc. The horizontal axis denotes the H I density at the centroid of the H I layer ($n_{\rm HI0}$) and the vertical axis denotes the scale-height ($z_{1/2}$).

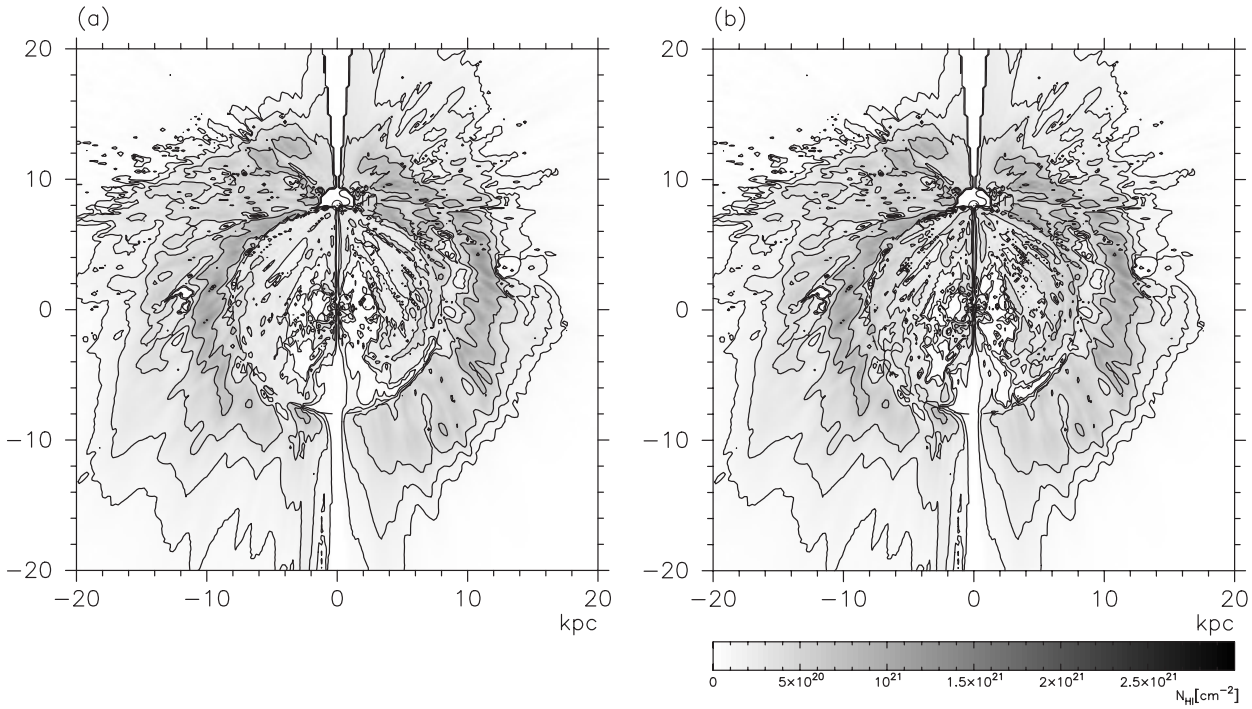

Fig. 13. (a) H I column density map derived by using a Gaussian function to determine the H I distribution in the inner Galaxy. (b) H I column density map derived with an exponential function. The contours are drawn at levels of 8.0×10^{19}, 1.6×10^{20}, 3.2×10^{20}, 6.4×10^{20}, and 1.3×10^{21} atom cm^{-2}.

4. *Fitting method* — We determined the H I distribution in the inner Galaxy by a fitting method, as mentioned in subsection 3.3. However, this fitting method cannot always work precisely. Largely deviated H I clouds from the surrounding gas, often seen in resultant maps, are thus doubtful, while a global feature is plausible.

5. *Dependence of adopted functions for z-distribution* — While the function $\mathrm{sech}^2(z)$ was adopted in our analysis, the real gas distribution can not be perfectly represented by it, because the gas is not isothermal (Lockman 1984). We present H I column density maps derived by using other functions, such as a Gaussian function and exponential function in figure 13. Though the resultant maps depend on the adopted functions, the global structure is not strongly affected by the difference of the chosen functions, but the resultant densities varies by a factor of ~ 2 inside the solar circle.

5. Summary

We obtained a three-dimensional H I distribution in the Milky Way Galaxy using the Leiden–Dwingeloo H I survey (Hartmann, Burton 1997), Parkes survey (Kerr et al. 1986), and the NRAO survey (Burton, Liszt 1983) by combining with Clemens (1985) and Dehnen and Binney (1998)'s rotation curves. The distance and density of H I clouds were determined by assuming that the Galaxy rotates circularly. We solved the near–far problem in the inner Galaxy using a fitting method based on a model of the vertical distribution (Spitzer 1942).

Our resultant map shows:

1. The Galaxy has three prominent spiral arms: the Outer arm, the Sagittarius–Carina arm, and the Perseus arm. All of the arms are logarithmic spiral arms.
2. The H I disk is strongly warping in the outer disk and the warping is asymmetric. Also, the inner disk is found to be tilting.
3. The size of the H I disk is about 17 kpc, and the H I mass within this radius is about $2.5 \times 10^9\, M_\odot$.
4. The H I disk is swelling in the southern hemisphere, which indicates that the Galaxy is significantly lopsided.
5. The scale-height increases with the radius globally. The scale-height is correlated with the H I volume density at the centroid of the H I layer.

This work was achieved by using the large H I survey data of Leiden–Dwingeloo northern hemisphere survey, Parkes southern hemisphere survey, and NRAO Galactic center survey. We would like to thank Dr. T. Sawada, Dr. J. Koda, and Dr. T. Handa for suggestions about writing the manuscript and for fruitful discussions.

References

Binney, J. 1992, ARA&A, 30, 51
Broeils, A. H., & van Woerden, H. 1994, A&AS, 107, 129
Burton, W. B. 1972, A&A, 19, 51
Burton, W. B., & Liszt, H. S. 1978, ApJ, 225, 815
Burton, W. B., & Liszt, H. S. 1983, A&AS, 52, 63
Burton, W. B., & te Lintel Hekkert, P. 1986, A&AS, 65, 427

Clemens, D. P. 1985, ApJ, 295, 422
Dehnen, W., & Binney, J. 1998, MNRAS, 294, 429
Diplas, A., & Savage, B. D. 1991, ApJ, 377, 126
Drimmel, R.,, & Spergel, D. N. 2001, ApJ, 556, 181
Georgelin, Y. M., & Georgelin, Y. P. 1976, A&A, 49, 57
Hartmann, D., & Burton, W. B. 1997, Atlas of Galactic Neutral Hydrogen (Cambridge: Cambridge University Press)
Honma, M., & Sofue, Y. 1997, PASJ, 49, 453
Kerr, F. J. 1969, ARA&A, 7, 39
Kerr, F. J., Bowers, P. F., Jackson, P. D., & Kerr, M. 1986, A&AS, 66, 373
Kulkarni, S. R., Blitz, L., & Heiles, C. 1982, ApJ, 259, L63
Lockman, F. J. 1984, ApJ, 283, 90
Malhotra, S. 1995, ApJ, 448, 138
Oort, J. H., Kerr, F. J., & Westerhout, G. 1958, MNRAS, 118, 379
Robin, A. C., Crézé, M., & Mohan, V. 1992, ApJ, 400, L25
Sanders, D. B., Solomon, P. M., & Scoville, N. Z. 1984, ApJ, 276, 182
Spitzer, L., Jr. 1942, ApJ, 95, 329
Swaters, R. A., Sancisi, R., & van der Hulst, J. M. 1997, ApJ, 491, 140
Verschuur, G. L. 1973, A&A, 22, 139
Weaver, H. 1970, in IAU Symp. 38, The Spiral Structure of Our Galaxy (Dordrecht: Reidel), 126